Chemically-oscillating reactions in the formation of botryoidal malachite

Dominic Papineau

London Centre for Nanotechnology, Department of Earth Sciences, and Center for Planetary Science, University College London, London, U.K.

Abstract

The origin of banding patterns in malachite [$Cu_2CO_3(OH)_2$] is an enduring problem in geology. While the bright green vivid colors of this mineral have been attributed to the presence of Cu, no specific process has been proposed that can explain the perfect circularly concentric banding and geometrical shapes in botryoidal malachite. These patterns of concentric equidistant laminations are comparable to those arising from chemically-oscillating experiments using the classical reactants of the Belousov-Zhabotinsky (B-Z) reaction. Through optical microscopy and micro-Raman imaging, this contribution documents that the geometric centers of the self-similar geometric patterns are often composed of organic matter. Carbon isotopes and trace elements further suggest that non-biological decarboxylation reactions of biological organic matter took place during diagenesis. Hence, the morphological and chemical characteristics of chemically-oscillating reactions offer a plausible explanation for the formation of botryoidal malachite and abiotic environmental decarboxylation reactions.

Keywords: Malachite, botryoids, Belousov-Zhabotinsky reaction, organic matter, Raman, decarboxylation

1. Introduction

Mineral banding is a common feature of mineral overgrowth during precipitation from aqueous solutions and microbial growth. Episodic growth leads to single crystals with concentric euhedral layers representing the age and composition of each generation of fluids, such as metamorphic zircons. However, this process does not predict that crystal habits or banding should have circularly concentric and radial geometries, such as in botryoidal malachite. The geometric shape of malachite can be modelled as a 'surface normal growth' phenomenon, based on a non-linear equation that plots cusps between smooth spheroids (Jettestuen et al., 2006). It has also been suggested that such geometric patterns grow heterogeneously, as a function of time, and influenced by some external processes triggering nucleation (Jamtveit and Hammer, 2012). While mathematical models can make progress, the enigma of the natural process leading to malachite banding and its occurrence as bunches of grapes is an enduring puzzle. This phenomenon is also relevant for biosignatures because stromatolite-like botryoidal growths commonly occur in malachite, yet their occurrence in nature is generally inconsistent with photic environments required for a photosynthetic microbial origin. In fact, botryoidal malachite generally occurs as crusts inside cavities in country rocks affected by supergene, briny, and Cu-rich fluids. Indeed, malachite is usually thought to be hydrothermal alteration or a secondary mineral developed from the weathering of other minerals. Yet, no theory fully explains the origin and shape of its distinct and notable banding.

At the start of the twentieth century, new diffusion experiments in silica gels showed the development of periodic layering due to diffusion, a pattern referred to as Liesegang banding

(Liesegang, 1910, 1915). The original idea put forward to explain the periodic colour layering was due to metal cation impurities diffusing in silica gel, which creates color gradients in objects like agate geodes (Liesegang, 1910). This phenomenon was subsequently proposed to explain banding in malachite (Hartman et al., 1934). Indeed, the appearance of Liesegang bands in silica gel is similar to some patterns exhibited by natural agates and chalcedony in geodes from volcanic terrains (Götze, 2011). However, most patterns in malachite and geodes are rounded as opposed to linear such as in Liesegang banding, hence this type of diffusion does not explain the geometry of botryoids. Therefore, current explanations for the origin of banding in malachite are incomplete.

The Belousov-Zhabotinsky reaction (B-Z reaction from hereon) is spontaneous under standard conditions and involves the oxidation of carboxylic acids (such as malonic acid – $C_3H_4O_4$) by a strong oxidizer and its corresponding halide salt (such as the oxidized halogen bromate and its halide salt bromide), as well as a strong acid (such as sulfuric acid; Belmonte, 1997; Orbán et al., 2001). When using metal-bearing redox-sensitive dye, such as ferroin (phenanthroline ferrous sulfate – $C_{12}H_8FeN_2O_4S$), this decarboxylation reaction becomes notable and unique as it produces characteristic self-similar patterns of circularly-concentric chemical waves (Zaikin and Zhabotinsky, 1970). Over minutes time scales, these chemical waves are displayed as blue-purple, circular, concentric and equidistant waves that propagate radially and periodically from randomly located spots in the orange-colored solution. Bubbles of CO_2 eventually form from the cleavage of carboxyl functional groups from malonic acid. Hence, the B-Z reaction is an out-of-equilibrium, spontaneous, cyclic, patterns-forming, and oxidation-reduction reaction. A new hypothesis can thus be posed for the origin of banding in malachite:

chemically-oscillating reactions participated in the formation of these enigmatic self-similar patterns. In this contribution, the botryoidal habit and geochemical composition of malachite are compared to the patterns and composition of chemically-oscillation reactions.

2. Materials and methods

2.1. Chemically-oscillating reactions

To study the detailed self-similar patterns of the B-Z reaction, more than sixty experiments performed in 10 cm diameter glass Petri dishes were imaged using the following reactants: 6 ml of (1M) $NaBrO_3$ mixed with (0.33M) H_2SO_4, 0.5ml of (1M) NaBr, 1ml of (1M) malonic acid, 1ml of (25mM) Ferroin (phenanthroline ferrous sulfate; Reagecon), and a drop of dilute triton X-100. The first three solutions are mixed until the yellow color disappears, which takes approximately 2 minutes of gentle stirring, and the ferroin redox indicator and dilute soap are then added. A bicolor orange-blue spontaneously forms upon contact with the solution and homogenization yields a first-order time-period oscillation of orange-blue colors for the entire Petri dish. If the solution is continuously stirred, the homogenized colored background will oscillate between orange-red and purple-blue, because stirring accelerates this longest time-period, and thus first-order, oscillation frequency. However, if the homogenous solution is left unstirred, a series of chemical waves diffuse through the solution and repeat over times scales of minutes until the Petri dish is filled with the blue color (typically after more than 20 minutes). Experiments were performed on countertops in ambient temperatures varying between about 20 and 25^{o}C most often in a fume hood and on an LED-illuminated light bench. The reaction is spontaneous and out-of-equilibrium and the pattern development lasts between about 45 and 75 minutes, depending on the number of resets (i.e. when the solution is gently stirred until the next

homogeneous orange background is re-established). Data was collected using various CCD cameras in both photo and video modes and only representative images are shown.

2.2. Comparative analyses of malachite botryoids by optical microscopy and micro-Raman

For the comparison of patterns in botryoidal malachite with those in the B-Z reaction, specimens in private collections were photographed and one was selected for petrographic analysis in thin section. Optical microscopy was thus performed on three thin sections of the botryoidal malachite from the Katanga locality in the Central African Copper Belt in the Democratic Republic of Congo. A BX-51 Olympus petrographic microscope located at UCL was used to collect transmitted and transmitted plus reflected images with the following objectives: 5x, 10x, 20x, 50x, and 100x. A condensing lens was used for all images. Oil immersion or ink markings were not used on the polished thin sections, which were cleaned by gently rubbing an acetone-wetted kimwipe.

A WITec α300 micro-Raman system at UCL was used to image organic matter in botryoidal malachite. Micro-Raman was performed using a 532 nm laser set at 8 mW, and according to previously described techniques (Papineau et al., 2011; 2016). An optic fiber of 50 microns in diameter was used to collect the inelastically-scattered photons, which were dispersed through a 600 l/mm grating, thus resulting in a spectral resolution of 4 cm^{-1}. The spatial resolution was set at one pixel per two microns, whereas the acquisition time on each pixel was 0.4 seconds, for a total of 84,100 spectra collected (290 x 290 pixels). Hyperspectral images are created using color-coded using the strongest unique peak of all phases present: malachite in green (filter center = 1495cm^{-1}, width = 20cm^{-1}), quartz in blue/purple (filter center = 466cm^{-1}, width = 30cm^{-1}), anatase in yellow (filter center = 143cm^{-1}, width = 25cm^{-1}), organic matter in

red (filter center = 1583cm^{-1}, width = 120cm^{-1}), and an unknown phase in dark red (filter center = 596cm^{-1}, width = 200cm^{-1}).

2.3. Bulk geochemical analyses of malachite

Powder of malachite was prepared using a steel mortar and pestle, which was prepared with the following steps: cleaned using soap and plastic brush, DI water rinses, acetone rinse, muffled quartz chips (600^{o}C for 4 hours in air) crushed to very fine powder, rinsed again with DI water, and finally air-dried. Malachite powder was transferred to muffled clear borosilicate glass vials (also 4 hours at 600^{o}C). Plastic caps were soaked in 10% HCl for 24 hours, followed by DI water rinses and air drying.

For bulk analysis of trace elements, ~0.1g of powder was initially heated in mixture of 1.0 ml hydrochloric acid (37% w/v; analytical grade), 1.0 ml nitric acid (69% w/v; analytical grade), and 0.5 ml hydrofluoric acid (40% w/v; analytical grade) at 110^{o}C for 16 hours. The solution was evaporated to incipient dryness before addition of 2.0 ml HNO_3 and 0.5 ml $HClO_4$ (70% w/v; analytical grade), which was again evaporated to incipient dryness. A further 1 ml aliquot of HNO_3 was evaporated and the residue dissolved in 100 ml of 1.0% HNO_3 prior to analyses by ICP-OES and ICP-MS at University College London. Data is reported in Table 2, which shows elemental abundances determined by ICP-OES as concentrations in ppm and % and by ICP-MS as concentrations in ppb. Analyses of certified reference material NBS120b (Florida Phosphate Rock) yielded recoveries above 95%. Bulk analyses of carbon isotopes were also performed at UCL using previously used techniques (Papineau et al., 2013), that included a Gas

Bench for bulk malachite carbonate and an Elemental Analyzer for organic matter in HCl-dissolved malachite, both linked to a Thermo Delta V isotope ratio mass spectrometer.

3. Results

3.1. Dimension and time-scale of patterns in chemically-oscillation reactions

Self-similar patterns are formed by the diffusion of reaction products, and these chemical waves are erased when they intersect each other through a process of destructive interference. It is noted however that typical patterns of destructive interference from interacting circular waves yield discontinuous circular wave lines (e.g. a double-slit diffraction pattern by a plane wave), whereas chemically-oscillating reactions are unique in showing that waves interfere destructively by erasing the wave trace at their intersection. Self-similar patterns in the B-Z reaction include the morphologies listed in (Table 1) and generally described as accumulations of myriad perfect, circularly-concentric, and equidistant laminations (Fig. 1a (pl. 2&3); Fig. 1e (pl. 1)). In most experiments, oxidation spots have circularly-concentric laminations that are only slightly imperfect with diameters spanning sub-millimeter to decimeter sizes (Fig. 1a (pl. 2); Fig. 1i (pl. 3)). Concentric spots can also have slightly imperfect equidistant or non-equidistant laminations (Fig. 1e (pl.2-3)), or they can be asymmetric irregular ellipses of chemical waves or with variable spacing distance (Fig. 1a (pl. 4)). Some chemical waves initiate from the edge of the Petri dish, which may be triggered by surface tension or invisible impurities on the borosilicate glass. This can lead to the formation of a cavity-shaped structure progressively closing outside-in (Fig. 1a (pl. 1)). Other notable and distinct morphological traits include parallel-layered to wavy patterns with intersecting oxidation spots (Fig. 1g (pl. 1&2)), columnar-turbinate (stromatolite-like) laminated patterns (Fig. 1g (pl. 4)), and strong color gradients in laminations can be associated

with a diffused spotted texture filling the orange background (Fig. 1g (pl. 3); Fig. 1i (pl. 1-2)). Rarely, oxidation spots display a globular texture where the spheroids have a pronounced color gradient rather than concentric circular laminations (Fig. 1c (pl. 1-4)).

Bubbles of CO_2 produced during these chemically-oscillating decarboxylation reactions generally remain attached to the Petri dish and grow over time to sizes more than 1mm in diameter (Fig. 1e (pl. 2)). The patterns change from one experiment to another, but they have the same self-similar characteristics as the concentric patterns described above: circularly-concentric waves that periodically expand radially and display a color gradient. Notably in several experiments, the spotted background oscillates with a different, faster, third-order time-period, distinct from the second-order chemical oscillations located in discrete oxidation spots (e.g. Fig. 1i (pl.1-2)). The oscillations in the blue and orange colors are thus represented by at least three orders of time periods: a first-order of pattern formation as completely filled with blue and reverting to its original orange background with a time-period on the order of about 20-30 minutes, a second-order of pattern formation with sub-millimetric to decimetric oxidation spots with chemical waves that have periods on the order of about 30 to 90 seconds, and lastly a third-order of pattern formation (present in less than about 10% of experiments) with sub-millimetric to millimetric spots or convex lined patterns that have periods on the order of 10 to 20 seconds.

3.2. Optical analysis of patterns in malachite botryoids

Botryoidal malachite exhibits randomly-located concentric spheroids with perfectly to imperfectly equidistant laminations with gradients of shades of green (Fig. 1b (pl. 1&2)). At the decimeter to millimeter scales, various polished cross-sections of malachite have these kinds of laminations that form spots with perfect to imperfect, merging lines of concentric laminations

that form concretionary cavity-structures or imperfect concentrically-layered spheroids (Fig. 1b (pl. 1-3)). This particularly distinguishing feature in self-similar patterns of malachite can also be described as cavity-shaped structures formed from the merging of rounded concentric waves that have had their trace erased through a process of destructive interference (Fig. 1f (pl. 2)). This important morphological characteristic of malachite has never been explained, yet it is identical to some features observed in chemically-oscillating reactions (Fig. 1e (pl. 4)). The laminations of malachite vary from perfect, circularly-concentric and equidistant laminations (Fig. 1f (pl. 1-3) and Fig. 1b (pl. 3)) to slightly imperfect, sub-rounded, non-equidistant laminations (Fig. 1b (pl. 1); Fig, 1h (pl. 3)). A particularly intriguing morphological features in malachite is the occurrence of convex-upward columnar-turbinate laminated pattern analogous to some columnar stromatolites (Fig. 1h (pl. 1)). Strong color gradients also occur in laminations that can be associated with diffused spotted texture (Fig. 1j (pl. 1)). Table 1 summarizes the similar morphological traits observed in cross-sections of malachite and in chemically-oscillating reactions.

When viewed in three dimensions, the malachite spheroids are generally of similar size and similar to grapes with spheroidally-concentric shells (Fig. 1d). Close examination under the optical microscope reveals geometrically perfect laminations that are sometimes truncated and discontinued. These appear as symmetric patterns with morphologies including perfectly concentric spots, open-book-like, and microscopic spherical rosettes (Fig. 1b, 1f, 1j). Self-similar macroscopic structures that emerge from these layers form columnar turbinate stromatolite-like structures, pillars with rounded-convex and hollow-concave ends, or outward-growing turbinate fans (Fig. 1h). When malachite forms linear layers, there are still perfect concentrically-layered

spheroids that span sizes between about 1 cm to ca. 0.1 mm (Fig. 1j). These spheroids form layers that grow inside rock cavities or on bedding planes. These observations demonstrate the existence of 3-D self-similar patterns in malachite that include circularly-concentric laminations, color gradients, randomly localized spots, and structures similar to rosettes, grapes, stromatolites, or cavities. Hence, the same kinds of self-similar patterns are observed in both in botryoidal malachite and in chemically-oscillating reactions.

3.3. Organic matter in malachite botryoids

Cross-sections of Katanga malachite reveal an abundance of fine perfectly equidistant laminations, sometimes with organic-rich layers (Fig. 2a) or forming turbinate columnar structures with color gradients varying from green to black-green (Fig. 2b-2c). Dendritic to arborescent opaque masses of organic matter are commonly located in the geometric center of malachite botryoids (Fig. 2d). Reflected light images reveal the occurrence of vugs inside the arborescent organic matter (Fig. 2e), whereas transmitted light images reveal laminations and bulbous protuberances (Fig. 2d, 2f). The bulbous protuberances also occur in the geometric center of smaller patterns of circularly-concentric laminations of carbonate (white arrows in Fig. 2f). The arborescent organic masses span sizes between about 500 to 1000 μm.

Micro-Raman imaging confirms the composition of organic matter with a poorly-resolved D1 peak at around 1345 cm^{-1} and a better-resolved G-peak at 1583 cm^{-1} (Fig. 2h) characteristic of low-grade metamorphic sedimentary organic matter such as kerogen. Raman spectra of organic matter show two types of crystallinity, with either a poorly-resolved or an unresolved D1 peak. This organic matter is also closely associated with layers more than 100 μm in thickness of another, unidentified phase with a broad peak at 596 cm^{-1}, possibly umber-like

(Fig. 2g). The spectra of organic matter are relatively noisy and there are no 2D peaks in the 2600-3000 cm^{-1} region, as would be expected from kerogen (Schopf and Kudryavtsev, 2009). The Raman spectrum of malachite shows medium intensity peaks for carbonate at 1062 and 1098 cm^{-1}, along with peaks at 218, 271, 348, 434, 537, 720, 752, and 1495 cm^{-1}, and the OH peak at 3382 cm^{-1} (Fig. 2h). This is similar to the peak distribution of Namibian malachite (rruff.info/malachite), which has peaks at 219, 268, 345, 431, 533, 717, 750, 1060 and 1095 cm^{-1}. Micro-Raman imaging also reveals the presence of anatase crystals a few microns in size inside the organic matter adjacent to the coarse-grained quartz at the root of the arborescent structure (Fig. 2g).

3.4 Bulk composition of Katanga malachite

Major elements in the Katanga malachite include Cu at 55.3% and P at 4.3% (Table 2). Trace elements are dominated by Al, Mn and Zn, which occur at concentrations of 401, 585, and 890 ppm, respectively (Table 2). Divalent cations such as Ba, Ca, Co, Cr, Fe, Mg, and Ni occur in concentrations of 40, 39, 200, 0.6, 85, 163, and 18 ppm, respectively. For halogens, I occurs in a concentration of 1.1 ppm, whereas Br is at 10.9 ppm. Rare Earth Elements (REE) occur in low concentration (total REE = 11.8 ppm) and form a trend of higher abundance for heavy REE and lower abundance for light REE. Lastly, the bulk malachite powder was found to contain organic matter with a $\delta^{13}C_{org}$ value of -28.6‰, in comparison with the carbonate which has a $\delta^{13}C_{carb}$ value of -10.6‰ and $\delta^{18}O_{carb\text{-}PDB}$ value of -5.1‰ (Table 2).

4. Discussion

4.1. From aqueous solution to mineralization

The following chemically-balanced equation represents the decarboxylation of malonic acid by reactants used in this work and some expected products:

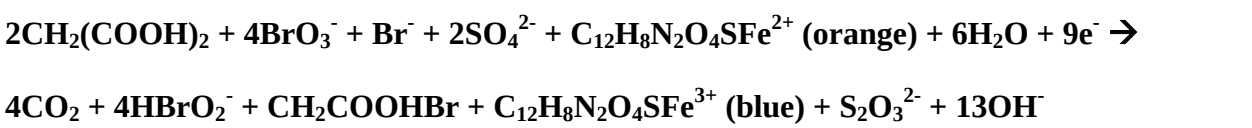

$$\mathbf{2CH_2(COOH)_2 + 4BrO_3^- + Br^- + 2SO_4^{2-} + C_{12}H_8N_2O_4SFe^{2+}\ (orange) + 6H_2O + 9e^- \rightarrow}$$

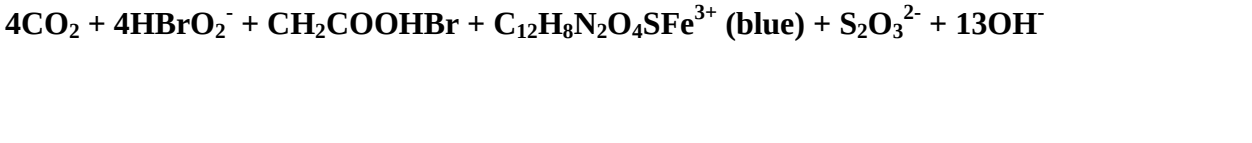

$$\mathbf{4CO_2 + 4HBrO_2^- + CH_2COOHBr + C_{12}H_8N_2O_4SFe^{3+}\ (blue) + S_2O_3^{2-} + 13OH^-}$$

This oxido-reduction reaction is catalyzed by redox-sensitive ferroin mediated by interaction between malonic acid and halogen compounds because halogens especially react with carboxyl groups in organic acids, leading to the formation of halogenated organic molecules. As carbon dioxide can precipitate carbonates at equilibrium under slightly alkaline pH, the above equation suggests that both CO_2 and alkalinity are created by the oxidation of malonic acid. Various intermediates are expected or predicted, such as bromomalonic acid ($CH_2COOHBr$), bromous acid ($HBrO_2$) and thiosulfate ($S_2O_3^{2-}$). Electrochemical analyses have demonstrated that a voltage potential exists between chemical waves and thus that an electron motive force is generated from chemically-oscillating reactions (Zhabotinsky, 1991). Measurements of Br^- concentration in the B-Z reaction also show that it varies in periodic oscillations and that the redox potential between the Br^- and BrO_3^- is 1.44 V (Körös and Orbán, 1978). This chemical potential acts to transfer electrons until either there are no more terminal electron acceptors (bromate and sulphate) or no more electron donor molecule (organic acids). The energy created by the reaction is responsible, in part, for the diffusion of reaction products away from oxidation spots, however the mechanisms of pattern initiation and development at the microscopic and nanoscopic scales remain to be documented. In nature, for as long as the solution pH is slightly alkaline and divalent cations are available in diagenetic pore water solutions, CO_2 could precipitate carbonate

minerals as micrite. Diffusing chemical waves with variable oxidation states could conceivably be immobilized in lithifying malachite micrite and contribute to the formation and crystallization of circularly-concentric and radially-aligned malachite crystals (e.g. Fig. 2d). For instance, gels of N-isopropylacrylamide and polyacrylamide-silica composites have been used with success to immobilize chemical waves in B-Z reactions (Chou Chen et al., 2011). It is therefore suggested that hydrated micritic malachite could allow diffusion of chemical waves, and lithification could immobilize them, although this still awaits experimental demonstration.

Experiments have shown that chemically-oscillating reactions can take place under variable ranges of reactant concentrations: 0.15-2.0 M H_2SO_4, 0.075-0.4 M $NaBrO_3$, and 0.05-0.8 M malonic acid (Körös and Orbán, 1978; Agladze et al., 1984; Belmonte et al., 1997). In fact, there are also various other organic acids that can be used for chemically-oscillating reactions including mono- and di-carboxylic acids and ketones (Belmonte et al., 1997; Orbán et al., 2001). Similarly, chemical oscillations have also been observed using various kinds of strong oxidizers such as iodate, bromate, and hydrogen peroxide (Briggs and Rauscher, 1972; Epstein et al., 1983). Several strong acids have also been used such as hypophosphite, arsenate, and sulfuric acid, and catalysts such as Mn^{2+}, Ce^{3+}, Fe^{2+}, Ru^{2+}, Cr^{2+}, Co^{2+}, $Fe(phen)_3^{2+}$ (ferroin), $Ru(bpy)_3^{2+}$ (ruthenium) have also been used to generate patterns in chemically-oscillating reactions (Belmonte et al., 1997; Orbán et al., 2001). In the Katanga malachite, most of these compounds occur (Table 2) and it is possible they could have contributed to chemical oscillations. The oxidation state of Cu in malachite is well-established to be +2 and Cu is a metal that can be halogenated by Br and I (Hemachandran and Chetal, 1986). Hence, since both Br and I occur in ppm levels in the Katanga malachite, a possible scenario could also involve Cu^{+1} and Cu^0 during diagenetic and supergene conditions, which could potentially contribute to the abiotic

decarboxylation of biomass. Unfortunately, in the absence of experimental evidence, the exact physical-chemical conditions during which botryoidal malachite forms are not known. Hence, the discussion shall now explore the similarities between the geometry of self-similar patterns in the chemically-oscillating reactions and in botryoidal malachite, and then focus on the organic matter in malachite.

4.2. On the origin of concentric fractal pattern morphologies

Self-similar patterns in chemically-oscillating experiments include cavity-shaped structures, perfectly to imperfectly circularly-concentric and equidistant laminations, columnar turbinate structures, color gradients in chemical waves, and various spotted, globular, zebra-striped, and fingerprint-like patterns (Table 1). The B-Z reaction is also known to produce spiral-like patterns inside concentric equidistant laminations (Agladze et al., 1984; Belmonte et al., 1997). Not all these patterns are documented in botryoidal malachite. For instance, no distinct spirals, zebra-striped or fingerprint-like patterns have been observed in malachite, in the knowledge of the author. However, the proliferation of spots in the B-Z reaction (Fig. 1i (pl. 1&2)) is reminiscent of the myriad small rounded concentric spots and rosettes found in botryoidal malachite (Fig. 1j (pl. 1&2)). In B-Z experiments, the zebra-pattern exhibited in association with turbinate columns (Fig. 1g, pl. 4) and the globular spots (Fig. 1c (pl. 1-3)) are morphologies akin to columnar turbinate pattern in stromatolitic malachite (Fig. 1h (pl. 1), 2b, 2c) and to grape-shaped malachite botryoids (Fig. 1d), respectively. Truncated and discontinuous laminations in the B-Z reaction (Fig. 1e (pl. 4)) are akin to those in malachite (Fig. 1f (pl. 1-2)) and can be explained by a process of destructive interference of radially-expanding chemical waves, which suggests that similar processes underlie the formation of such structures.

Circularly-concentric, equidistant laminations with color gradients and sizes between sub-millimeter to decimeter in B-Z experiments (Fig. 1a (pl. 2), 1e (pl. 1); 1i (pl. 3)) are identical to perfectly concentric malachite spheroids from decimetric botryoids to microscopic rosettes (Fig. 1b (pl. 1), 1d (pl. 2), 1f (pl. 3), 1j (pl. 2-3)). In summary, there are several forms of self-similar patterns in chemically-oscillating reactions that share morphologies identical to those in botryoidal malachite.

Mathematically, the changing patterns in chemically-oscillating reactions can be described using well-known equations such as Euler's formula (including Euler's identity), Fourier transform, the Navier-Stokes equation, and the wave equation. The Navier-Stokes equations illustrate the motion of viscous fluid substances, and they have been used to model fluid flow and diffusion processes like the B-Z reaction (Kitahata et al., 2002). Spherical waves oscillating from point sources can be represented by an n-dimensional wave equation: for the B-Z reaction, that partial differential equation would describe the time-dependent scalar function of particle motion in 3-D space as an oscillating function from randomly located point sources. The periodicity or frequency of the chemical waves is related to time through Fourier transform. Lastly, Euler's identity ($e^{i\pi} + 1 = 0$) is an ideal solution to Euler's formula, which equates a unit complex number ($e^{i\varphi}$) to the trace of a unit circle in a complex plane. It can then be suggested that these equations might have a solution related to the types of geometries and periodic oscillations observed in both the B-Z reaction and in malachite botryoids. One also needs to consider the fact that many forms in nature can be described by fractals and that mathematical models of B-Z geometric patterns are complex. Minerals are a fundamental type of fractal where the unit cell repeats over several dimension scales in a geometric pattern defined by 4 polygonal shapes (with 2, 3, 4, or 6 sides), 14 Bravais lattices, 32 point groups, and 230 space groups.

Mathematical fractals might form botryoidal chalcedony through Mandelbrot-like pattern growth (Brasier et al., 2005), manganiferous dendrites have been modelled as two-dimensional Laplacian-type growth fractals (Garcia-Ruiz, 1994; Seilacher, 2001), and deep-sea stromatolitic manganese nodules can be modelled as fractal aggregates of polyhedra (Akai et al., 2013). Future work should compare the mathematical modelling of patterns in chemically-oscillating reactions with those in malachite.

While mathematics constitutes one approach to contribute to the problem of the origin of botryoidal malachite, this mineral has also not yet been experimentally synthesized in the laboratory. Low-temperature supergene conditions have been inferred from the mode of occurrence of malachite in rocks. The exact formation process remains unknown, but it could have involved some of the metals detected in the bulk composition such as Cu, P, Zn, Mn, Co, and V, because these can all have variable oxidation states and they are all relatively abundant in the Katanga malachite. In addition, the presence of bromine and iodine in malachite is consistent with these compounds having been involved in its formation. This new information could be useful for future malachite synthesis experiments under supergene-like low-temperature conditions.

4.3. Organic matter from biomass as a reactant in geological chemically-oscillating reactions

New observations by optical microscopy and micro-Raman imaging of malachite from Katanga show the occasional presence of organic matter located in the geometric centers of concentric features (Fig. 2d-2f). This organic matter is highly heterogeneous in the bulk rock and has a $\delta^{13}C_{org}$ value of -28.6‰ consistent with biological fractionation, whereas bulk malachite

has a $\delta^{13}C_{carb}$ value of -10.6‰ consistent with the oxidation of organic matter. In fact, similar ^{13}C-depleted compositions for organic matter and carbonate are common in sedimentary concretions and in banded iron formations where they are thought to represent oxidized biomass (Plet et al., 2016; Dodd et al., 2019). Hence, the C-isotope compositions of organic matter and carbonate in the Katanga malachite are independent signatures for the decarboxylation and oxidation of biomass. This is also akin to some agate geodes that have comparable, circularly-concentric, and self-similar patterns as well as bitumen (Gaweda and Rzymelka, 1992). Agate geodes also have ^{13}C-depleted carbonate (Götze et al., 2015; 2011), and/or have various volatile compounds as fluid inclusions including NO, SO, CO_3^{2-}, CH, and HF (Richter-Feig et al. 2018). The latter signatures in agate geodes can thus also be used to suggest that inorganic acids contributed to produce ^{13}C-depleted carbonate during the oxidation of ^{13}C-depleted organic acids. Organic matter of biological origin and inside concretions is usually rich in -COOH groups, which are known to be removed through decarboxylation during diagenesis and metamorphism (Bernard et al., 2007). This source of CO_2 is thus ^{13}C-depleted and can mix with variable amounts of seawater carbonic acid. The petrographic relationship between the organic matter and botryoids is consistent with the interpretation that the organic matter was decarboxylated in oxidizing and Cu-rich fluids. Lastly, the co-occurrence of anatase in the dendritic organic matter is also consistent with other reports of the presence of TiO_2 with fossil biomass, including in Paleoarchean botryoids and stromatolites (Djokic et al., 2017), and Paleoproterozoic microfossiliferous apatite granules (Papineau et al., 2017).

The **a**rborescent masses of organic matter in malachite are similar to structures referred to as *Frutexites*. *Frutexites* microfossils often appear to be associated with evidence for the putrefaction of biomass, such as their bulbous arborescent growth directly onto animal fossils.

For instance, *Frutexites* are seen in Cretaceous brachiopods, bivalves, belemnites, and ostracods from Norfolk in the United Kingdom (Andrews et al., 2015), Jurassic foraminifera from the Betic-Rifian Cordillera in Spain (Reolid, 2011), and Devonian rugose corals from the eastern Anti-Atlas in southern Morocco (Jakubowicz et al., 2014). These microbial structures also occur in Late Paleoproterozoic stromatolites from Western Ontario in Canada (Walter and Awramik, 1979), and in modern concretionary structures of zeolite from the Mariana Trench seafloor (Peng et al., in review). *Frutexites* are commonly dominated by organic matter and modern examples have been found to contain DNA from various kinds of Bacteria and Archaea, many of which are involved in the N-cycle (Heim et al., 2017; Peng et al., in review). Phosphorous is a vital element for life and is found in high abundance in the Katanga malachite (Table 2), which is analogous to the presence of biological apatite that forms diagenetic rosettes with organic matter, carbonate, and quartz in Paleoproterozoic stromatolitic phosphorite (Papineau et al., 2016). Hence, high P in the Katanga malachite is further evidence for a biological origin of the organic matter that constitutes the arborescent structures. The new structures of organic matter that form arborescent morphologies in the geometric centers of Katanga malachite botryoids are therefore analogous to similar structures seen in deep-sea, deep crustal, and diagenetic settings. However, because malachite botryoids form in concretionary cavity structures from surface groundwater solutions in the absence of light, stromatolite morphologies in botryoidal malachite are unlikely to be evidence for phototrophy. Nevertheless, their occurrence in botryoidal crust is consistent with the non-biological decomposition and decarboxylation of biological organic matter and this occurrence in concretionary structures is another possible link with chemically-oscillating reactions.

5. Implications

The similarities between perfect patterns in chemically-oscillating reactions and those in botryoidal malachite are visually striking. Chemically-oscillating reactions produce self-similar patterns of circularly-concentric laminations spanning sizes between hundreds of microns to decimeter scales, identical to the shapes and size range of botryoidal malachite, which contains microscopic rosettes and macroscopic botryoids. Because these patterns are self-similar and span several orders of size dimensions, they can be referred to as fractal patterns. The geometric centers of malachite botryoids often contain dense arborescent or bulbous dendritic organic matter, which is implied as a major source of reactants, especially carboxyl, during the chemical oscillations. Depending on the availability of oxidants and halogens, chemically-oscillating reactions could occur spontaneously as a result of diagenetic biomass decomposition and its decarboxylation. Decarboxylation would occur during the putrefaction of biomass, which produces CO_2 and could have mixed with other sources of carbonate (such as seawater) to then precipitate as malachite. This could conceivably occur rapidly after a rise in alkalinity and freeze instantly after the passage of chemical waves. Chemically-oscillating reactions require organic acids of biological or non-biological origin, produce CO_2 bubbles and thus contribute to the carbon cycle. Therefore, botryoidal malachite and probably various other spheroidally-concentric sedimentological structures likely constitute signatures of decarboxylation reactions in aqueous environments. If sedimentological features do indeed arise from chemically-oscillating reactions, such signatures could be found to be ubiquitous during some periods of Earth history, for instance during the Paleoproterozoic, Neoproterozoic, and Late Paleozoic-Mesozoic, when environmental O_2 levels significantly increased, as well as on other ancient planetary surfaces as evidence of possible prebiotic chemical reactions.

438

439 **6. Acknowledgements**

440 I acknowledge fruitful discussions on this topic with Z. She, K. Devine, J. Götze, G.
441 Shields, N. Lane, E. Oelkers, R.M. Hazen, J. Cleaves, M. Chan, and T. Kee as well as continuing
442 support from the LCN and UCL. Z. She and B. Shen are acknowledged for preparing solutions
443 and providing preliminary trace element analyses. A.-L. Jourdan performed stable isotope
444 analyses and G. Tarbuck conducted ICP-MS and ICP-OES analyses, both of whom are gratefully
445 acknowledged. J.M. McArthur and two anonymous reviewers are kindly thanked for constructive
446 comments that improved this manuscript.

447

448

449 **7. References**

450

451 Agladze, K.I., Krinsky, V.I., and Pertsov, A.M. (1984) Chaos in the non-stirred Belousov-
452 Zhabotinsky reaction is induced by interaction of waves and stationary dissipative
453 structures. *Nature* **308,** 834-835.

454 Akai, J., Akiyama, S., Tsuchiyama, A., and Akai, K. (2013) Ocean manganese nodules as
455 stromatolite with a fractal like-signature. *Physics and Chemistry of the Earth* **58-60,** 42-
456 48.

457 Andrews, J.E., Kendall, A.C., and Hall, A. (2014) Microbial crusts with Frutexites(?) and iron
458 staining in chalks: Albian-Cenomanian boundary, Hunstanton, UK. *Geological Magazine*
459 **152,** 1-11. DOI: 10.1017/S0016756814000107

Belmonte, A. Ouyang, Q., and Flesselles, J.-M. (1997) Experimental survey of spiral dynamics in the Belousov-Zhabotinsky reaction. *Journal de Physique II, EDP Sciences* **7,** 1425-1468.

Bernard, S., Benzerara, K., Beyssac, O., Menguy, N., Guyot, F., Brown, G.E. Jr., and Goffé, B. (2007) Exceptional preservation of fossil plant spores in high pressure metamorphic rocks. *Earth and Planetary Science Letters* **262,** 257-272.

Brasier, M.D., Green, O.R., Lindsay, J.F., McLoughlin, N., Steele, A., and Stoakes, C. (2005) Critical testing of Earth's oldest putative fossil assemblage from the ~3.5 Apex chert, Chinaman Creek, Western Australia. *Precambrian Research* **140,** 55-102.

Briggs, T.S. and Rauscher, W.C. (1973) An oscillating iodine clock. *Journal of Chemical Education* **50,** 496.

Chou Chen, I., Kuksenok, O., Yashin, V.V., Moslin, R.M., Balazs, A.C., and Van Vliet, K.J (2011) Shape- and size-dependent patterns in self-oscillating polymer gels. *Soft Matter* **7,** 3141-3146.

Djokic, T., Van Kranendonk, M.J., Campbel, K.A., Walter, M.R., and Ward, C.R. (2017) Earliest signs of life on land preserved in ca. 3.5 Ga hot spring deposits. *Nature Communications.* DOI: 10:1038/ncomms15263.

Dodd, M.S., Papineau, D., She, Z., Manikyamba, C., Wan, Y., O'Neil, J., Karhu, J., Rizo, H., Pirajno, F. (2019) Widespread occurrences of variably crystalline ^{13}C-depleted graphitic carbon in banded iron formations. *Earth and Planetary Science Letters* **512,** 163-174.

Epstein, I.R., Kustin, K., De Kepper, P., and Orbán, M. (1983) Oscillating chemical reactions. *Scientific American*, 112-123.

Garcia-Ruiz, J.M., (1994) Inorganic self-organisation in Precambrian cherts. *Origins of Life and Evolution of the Biosphere* **24,** 451-467.

Gaweda, A. and Rzymelka, J.A. (1992) Bituminous agates from rhyolites in the environs of Nowy Kosciol, Lower Silesia. *Mineralogia Polonica* **23,** 73-84.

Götze, J. (2011) Agate – fascination between legend and science. In: Zenz, J. (ed.) Agates III. Bode-Verlag, 19-133.

Götze, J., Möckel, R., Vennemann, T., and Müller, A. (2015) Origin and geochemistry of agate in Permian voclanic rocks of the Sub-Erzgebirge basin, Saxony (Germany). *Chemical Geology* **428,** 77-91.

Hartmnan, R.J., Kanning, E.W., and Klee, F.G. (1934) The Liesegang phenomenon applied to banded malachite. *Journal of Chemical Education* **11,** 346-350.

Heim, C., Quéric, N.-V., Ionescu, D., Schafer, N., and Reitner, J. (2017) Frutexites-like structures formed by iron oxidizing biofilms in the continental subsurface (Äspö Hard Rock Laboratory, Sweden) *PLOS One.* DOI: 10.1371/journal.pone.0177542

Hemachandran, K. and Chetal, A.R. (1986) X-ray K-absorption study of copper in malachite mineral. *Phys. Stat. Sol.* **136,** 181-185.

Jakubowicz, M., Belka, Z., and Berkowski, B. (2014) Frutexites encrustations on rugose corals (Middle Devonian, southern Morocco): complex growth of microbial microstromatolites. *Facies* **60,** 631-650.

Jamtveit, B. and Hammer, Ø (2012) Sculpting of rocks by reactive fluids. *Geochemical Perspectives* **1,** 341-480

Jettestuen, E., Jamtveit, B., Podladchikov, Y.Y., deVilliers, S., Amundsen, H.E.F., and Meakin, P. (2006) Growth and characterization of complex mineral surfaces. *Earth and Planetary Science Letters* **249,** 108-118.

Körös, E. and Orbán, M. (1978) Uncatalysed oscillatory chemical reactions. *Nature* **273,** 371-372.

Lazar, I., Gradinaru, M., and Petrescu, L. (2013) Ferruginous microstromatolites related to Middle Jurassic condensed sequences and hardgrounds (Bucegi Mountains, Southern Carpathians, Romania). *Facies* **59,** 359-390.

Liesegang, R.E. (1910) Die Entstehung der Achate. *Zentralblatt für Mineralogie* **11,** 593-597.

Liesegang, R.E. (1915) Die Achate. Verlag von Theodor Steinkopff, Dresden und Leipzig, 122 S.

Orbán, M., Kurin-Csörgei, K., Zhabotinsky, A.M., and Epstein, I.R. (2001) A new chemical system for studying pattern formation: Bromate-hypophosphite-acetone-dual catalyst. *Faraday Discussion* **120,** 11-19.

Papineau, D., She, Z., and Dodd, M.S. (2017) Chemically-oscillating reactions during the diagenetic oxidation of organic matter and in the formation of granules in late Paleoproterozoic chert from Lake Superior, *Chemical Geology* **470,** 33-54.

Papineau, D., De Gregorio, B.T., Fearn, S., Kilcoyne, D., Purohit, R., and Fogel, M.L. (2016) Nanoscale petrographic and geochemical insights on the origin of Paleoproterozoic stromatolitic phosphorites from Aravalli, India. *Geobiology* **14**, DOI: 10.1111/gbi12164. 3-32.

Papineau, D., DeGregorio, B.T., Cody, G.D., O'Neil, J., Steele, A., Stroud, R.M., and Fogel, M.L. (2011) Young poorly crystalline graphite in the >3.8 Gyr old Nuvvuagittuq banded iron formation, *Nature Geoscience* **4,** 376-379.

Peng, X. Guo, X., Czaja, A., and Papineau, D. (*in review in Science Advances*) Endolithic life in metamorphic ocean crust. 24 pp.

Plet, C., Grice, K., Pages, A., Ruebsam, W., Coolen, M.J.L., and Schwark, L. (2016) Microbially-mediated fossil-bearing carbonate concretions and their significance for paleoenvironmental reoncstructions: A multi-proxy organic and inorganic geochemical appraisal. *Chemical Geology* **426,** 95-108.

Richter-Feig, J., Möckel, R., Götze, J., Heide, G. (2018) Investigation of fluids in microcrystalline and microcrystalline quartz in agate using thermogravimetry-mass-spectrometry. *Minerals* **8,** 72. DOI: 10.3390/min8020072.

Schopf, J.W. and Kudryavtsev, A.B. (2009) Confocal laser scanning microscopy and Raman imagery of ancient microscopic fossils. *Precambrian Research* **173,** 39-49.

Seilacher, A. (2001) Concretion morphologies reflecting diagenetic and epigenetic pathways. *Sedimentary Geology* **143,** 41-57.

Turing, A.M. (1952) The chemical basis of morphogenesis. *Phil. Trans. Royal. Soc. London* **237,** 37-72.

Walter, M.R. and Awramik, S.M. (1979) Frutexites from stromatolites of the Gunflint iron formation of Canada, and its biological affinities. Precambrian Research 9, 23-33.

Zhabotinsky, A.M. (1991) A history of chemical oscillations and waves. *Chaos* **1,** 379-386.

Zaikin, A.N. and Zhabotinsky, A.M. (1970) Concentration wave propagation in two-dimensional liquid-phase self-oscillating system. *Nature* **225**, 535.

Figure 1: Morphological comparison of sub-millimetric to decimetric self-similar patterns in chemically-oscillating experiments (left, orange-blue coloured liquid in one-decimetre diameter Petri dishes) and in botryoidal malachite (right, various specimens from private collections). In B-Z experiments, none of the patterns were induced, e.g. with a tool. a-b) cavity shapes with imperfect to perfect concentric equidistant laminations associated with spheroidal to ellipsoidal concentric spots, c-d) globular growth patterns without or with few concentric laminations and sometimes with zebra-like bands (white arrows), e-f) spots with perfect to slightly imperfect equidistant laminations (yellow arrows show CO_2 bubbles), g-h) linear to wavy and columnar turbinate (stromatolite-like) equidistant laminations showing colour gradients along chemical waves and laminations as well as spotted patterns (white arrows), i-j) spotted pattern (white arrow) in background (with a

second-order oscillation and inverted textures in the B-Z reaction) and with perfect to imperfect concentric laminations from the micrometre to centimetre scales.

Figure 2: Petrographic context of organic matter with bulbous dendritic morphology located in the geometric centre of self-similar malachite botryoids. a-c) Transmitted light images through thin sections showing the location of *Frutexites* (black organic matter in red boxes) and the turbinate-like stromatolite textures of green to black malachite from Katanga. d) opaque organic matter in the centre of radiating acicular malachite, e) transmitted and reflected light image of dendritic organic matter with cavities located in the geometric centre of concentric malachite laminations, f) dendritic and layered organic matter located in the geometric centres of several concentrically-laminated spots of malachite (white arrows), g) micro-Raman image of the organic matter in (f) associated with quartz and anatase, h) Raman spectra of the minerals shown in (g) showing two types of organic matter.

Table 1: comparison of morphological traits between the self-similar patterns in malachite and in chemically-oscillating reactions.

Morphological trait	Chemically-oscillating reaction	Malachite
Circularly concentric and equidistant laminations	Fig. 1a (pl. 2, 3,) and Fig. 1e (pl. 1, 2)	Fig. 1b (pl. 1-3) and Fig. 1f (pl. 1-3)
Spots with concentric equidistant laminations spanning sizes from sub-millimeter to decimeter	Fig. 1a (pl. 2) and Fig. 1i (pl. 3)	Fig. 1b (pl. 2) and Fig. 1j (pl. 3)
Cavity-shaped structures formed from the destructive interference of chemical waves	Fig. 1a (pl. 1, 3)	Fig. 1b (pl. 2)
Asymmetric (sub-ellipsoidal) concentric laminations	Fig. 1a (pl. 1, 4), Fig. 1e (pl. 3), and Fig. 1i (pl. 4)	Fig. 1b (pl. 1, 3) and Fig. 1h (pl. 3)
Parallel-layered to wavy patterns with intersecting oxidation spots	Fig. 1g (pl. 1, 2)	Fig. 1f (pl. 1) and Fig. 1j (pl. 1-3)
Columnar-turbinate laminated pattern (stromatolite-like)	Fig. 1g (pl. 4.)	Fig. 1h (pl. 1-3)
Colour gradients in laminations	Fig. 1c (pl. 3, 4) and Fig. 1g (pl. 3)	Fig. 1b (pl. 1-3) and Fig. 1j (pl. 1)
Diffused spotted texture with a distinct periodicity than laminations	Fig. 1i (pl. 1, 2)	Fig. 1h (pl. 3) and Fig. 1j (pl.1-3)
Globular texture with three-dimensional grape-like morphology	Fig. 1c (pl. 1-4)	Fig. 1d (pl. 1-3)

Table 2: Bulk geochemical composition of Katanga malachite*

	ppb	ppm	%
Al		401.50	
As		33.28	
Ba		39.81	
Be	11274.0		
Bi	4.8		
Ca		38.88	
Cd	1.0		
Co	199466.9		
Cr	561.7		
Cu			55.27
Fe		85.05	
K		75.23	
Mg		163.28	
Mn		585.36	
Na		24.07	
Ni		17.97	
P			4.28
Pb		3.44	
Ti		6.91	
V		171.55	
Zn		890.94	
Sc	1907.9		
Y	6657.0		
La	369.7		
Ce	343.5		
Pr	136.2		
Nd	761.6		
Sm	363.2		
Eu	122.1		
Gd	732.9		
Tb	137.5		
Dy	889.3		
Ho	197.0		
Er	544.2		
Tm	71.5		
Yb	455.9		
Lu	73.1		
Th	313.7		
Br	10864.8		
I	1102.7		
$\delta^{13}C_{carb}$	-10.6‰		
$\delta^{18}O_{carb\text{-}PDB}$	-5.1‰		
$\delta^{13}C_{org}$	-28.6‰		

* Concentrations in ppb are from the ICP-MS while those in ppm and % are from the ICP-OES.

a)

b)

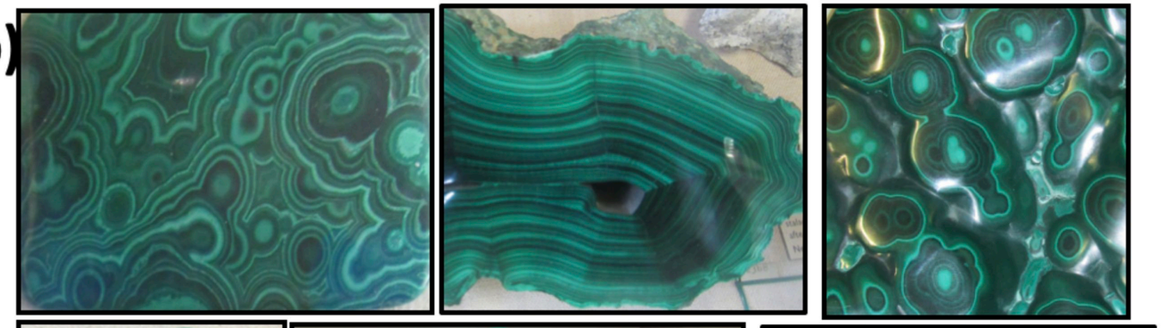

c)

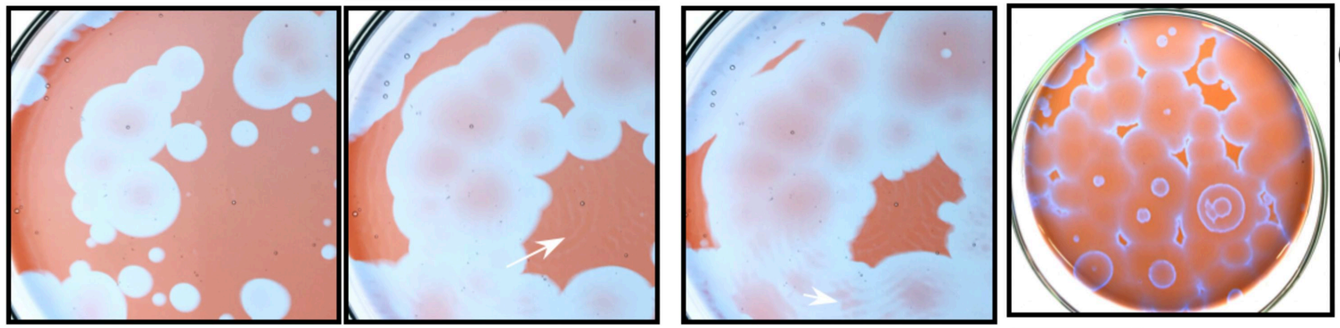

d)

e)

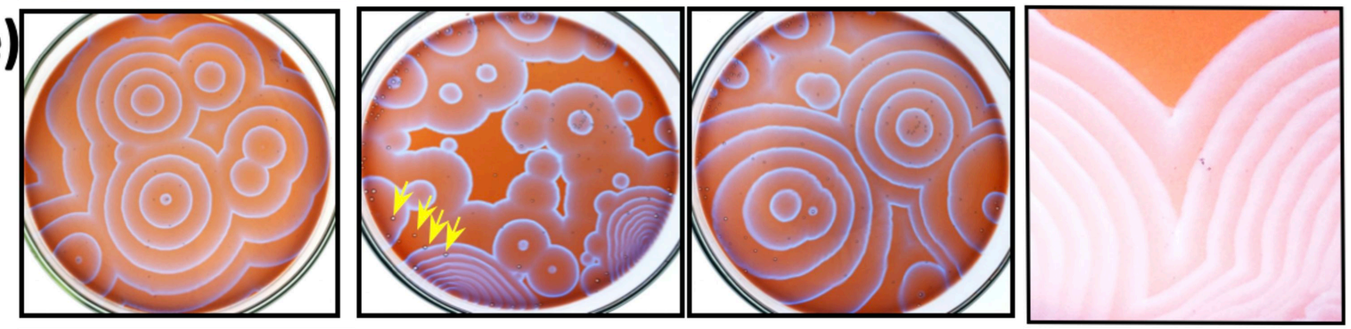

f)

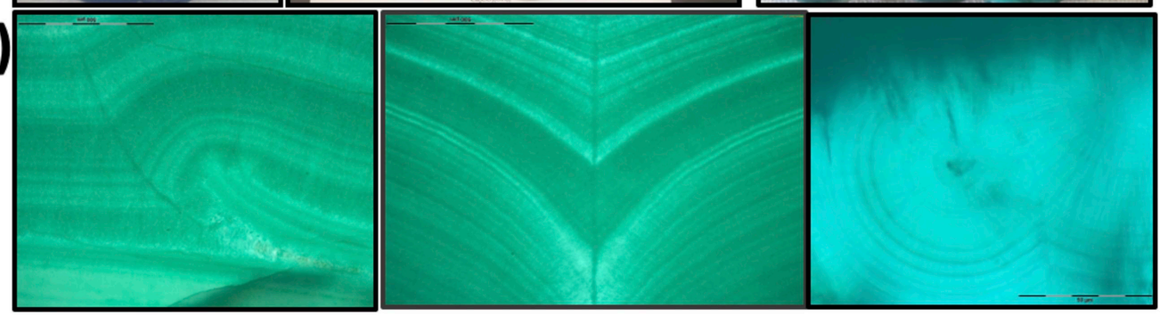

g)

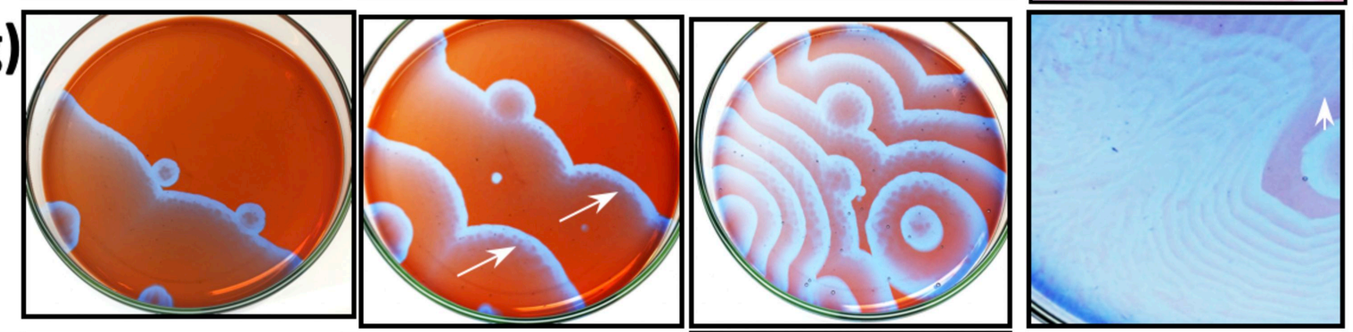

h)

i)

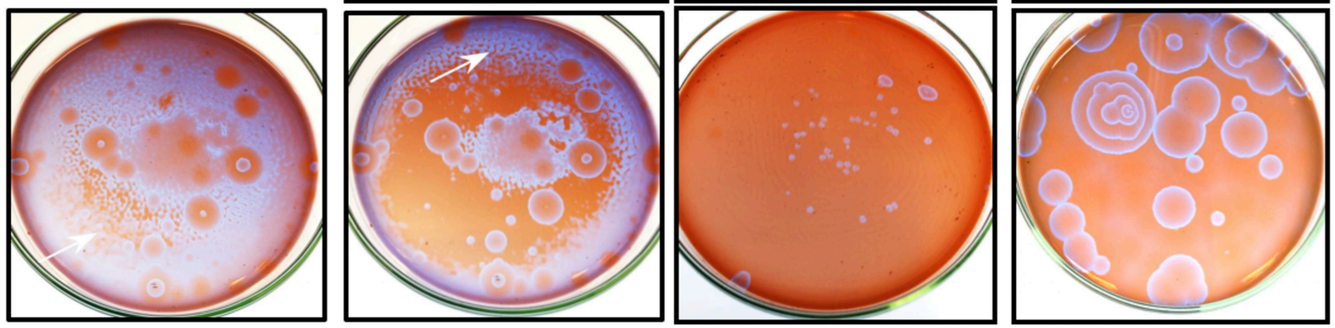

j)

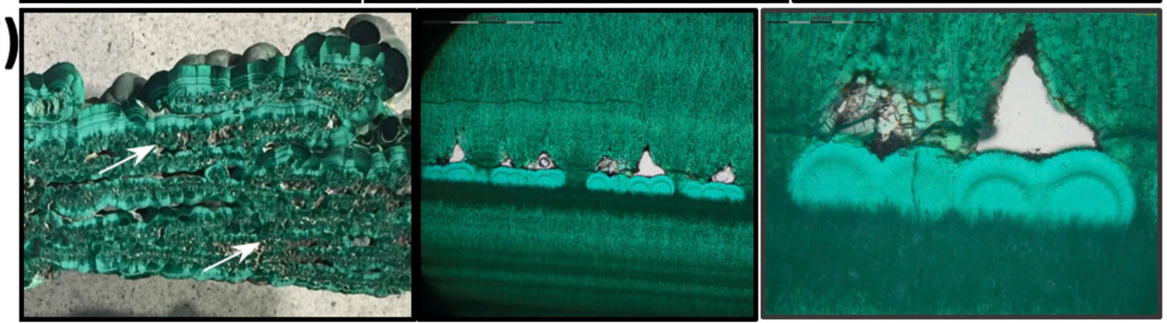

a)

b)

c)

1 cm

d)

e)

organic matter

f)

organic matter

g)

malachite

organic matter

organic matter

quartz

anatase

100 µm

h)

218 271 434 466 537 596 638 720 752 1062 1098 1322 1368 1495 1583 3382

348 1345

143

malachite

quartz

anatase

unknown (umber?)

organic matter 1

organic matter 2

500 1000 1500 2000 2500 3000 3500

Wavenumber (cm^{-1})